Z. Phys. C - Particles and Fields 33, 125-133 (1986)

Zeitschrift für Physik C Particles and Fields


# Renormalization Scheme Dependence of Electroweak Radiative Corrections

W. Hollik and H.-J. Timme

II. Institut für Theoretische Physik der Universität, D-2000 Hamburg, Federal Republic of Germany

Received 7 August 1986

**Abstract.** We compare two renormalization schemes of the electroweak standard model: the on-shell scheme with $e$, $M_W$, $M_Z$, $M_H$, and the fermion masses $\{m_f\}$ as free parameters, and an intermediate scheme where the $W$ boson self energy is renormalized at $q^2=0$ instead of $q^2=M_W^2$. The $M_W-M_Z$ interdependence, and the differential $e^+e^-\to\mu^+\mu^-$ cross section including polarized beams are calculated in both schemes to one-loop order. We find striking differences between the forward-backward asymmetries and the polarization asymmetries near the $Z$ resonance after inclusion of weak and QED corrections.

## 1. Introduction

Predictions of the electroweak standard model [1] have been confirmed by the discovery of the $W$ and $Z$ bosons with the expected masses [2]. The next step of precision tests of the standard model beyond the tree level requires theoretical predictions which are normally based on perturbative calculations of radiative corrections. The renormalizability of the model [3] ensures that this is possible by multiplicative renormalization. Radiative corrections have been calculated to one-loop order for various processes: low energy processes ($\mu$ lifetime, $\nu$ scattering) [4-9] and high energy $e^+e^-$ annihilation [10, 11]. For calculations beyond the tree level it is necessary to specify a renormalization scheme, which defines
- the free parameters in the Lagrangian,
- the renormalization conditions in order to express the bare parameters and fields in terms of the renormalized ones,
- the connection of the free parameters with the experimental input data.

One can distinguish between three types of renormalization schemes applied in electroweak loop calculations:

*(i)* The on-shell scheme [4-6, 12] makes use of the masses $M_W$, $M_Z$, $M_H$, $\{m_f\}$ of the massive vector bosons, the scalar Higgs boson, and fermions as free parameters. The renormalization conditions fix the finite parts of the renormalization constants in a way that directly allows for the particle content of the theory. Besides the masses, $e=\sqrt{4\pi\alpha}$ ($\alpha$ being the electromagnetic fine-structure constant) is commonly used as a precisely measured coupling constant.

*(ii)* Instead of the gauge boson masses $M_W$ and $M_Z$, the renormalization can be based on the use of low energy parameters $G_F$ and $\theta_W$, where $G_F$ is the $\mu$ decay constant and $\theta_W$ the weak mixing angle measured e.g. in $\nu_\mu e/\bar{\nu}_\mu e$ scattering [7, 8]. The renormalization conditions ensure that $G_F^2$ determines the $\mu$ lifetime $\tau_\mu$ and $\sin^2\theta_W$ the contribution of electromagnetic current to the weak neutral current. $M_W$ and $M_Z$ then can be derived by determination of the poles of the corresponding renormalized propagators.

*(iii)* The $\overline{\text{MS}}$ scheme [9] has the advantage that all the renormalization constants are fixed by the simple prescription of subtracting the singular parts of the two- and three-point functions. However, after relating the parameters $\alpha(\mu)$, $m_W(\mu)$, $m_Z(\mu)$, $m_H(\mu)$, and $\{m_f(\mu)\}$ to the corresponding physical quantities, this scheme becomes as complicated as (i) and (ii) [13].

For a survey see [14].

Due to the renormalization group invariance all renormalization schemes are equivalent. However, as long as we can only approximate physical observ-

ables by perturbative calculations these approximations are renormalization scheme dependent: the results in a fixed order given in different schemes deviate from each other by higher order contributions. This, however, does not mean a quantitative numerical estimate. Consequently, for testing the reliability of electroweak one-loop calculations, different renormalization schemes have to be compared with respect to their numerical predictions for measurable quantities.

The intention of this paper is to investigate the size of the renormalization scheme effect in the calculation of one-loop corrections to the following observables:

(a) the relation between the masses $M_W$ and $M_Z$,

(b) the cross section and forward-backward asymmetry in $e^+e^- \to \mu^+\mu^-$,

(c) and the longitudinal polarization asymmetry in $e^+e^- \to \mu^+\mu^-$.

To be concrete, we select two different renormalization schemes (RS1 and RS2), perform systematically the renormalization procedure, and compare the (a), (b), and (c) results obtained in both schemes.

These schemes are characterized as follows:

RS1: The free parameters are chosen as $e$, $G_F$, $M_Z$, $M_H$, $\{m_f\}$. The renormalization conditions are the on-shell conditions for $M_Z$, $M_H$, $\{m_f\}$, but not for $M_W$. Instead, the $W$ boson self energy is renormalized at zero momentum transfer such that $\tau_\mu$ is determined by $G_F$ in the same way as in the Fermi theory. $M_Z$ will be measured in near future with a precision of at least 50 MeV at LEP/SLC [15]. Together with $e$ and $G_F$, this scheme directly contains those quantities which are known with best precision as free parameters. The physical $W$ mass $M_W$ is predicted by the pole (real part) of the renormalized $W$ propagator. Since this scheme is a mixture of the types *(i)* and *(ii)* we shall also call it the "intermediate scheme".

RS2: This is the on-shell scheme with the free parameters $e$, $M_W$, $M_Z$, $M_H$, $\{m_f\}$. Now the on-shell condition is also imposed on the $W$ self energy. The value for $M_W$ can be related to the other parameters by calculating $\tau_\mu(e, M_W, M_Z, M_H, \{m_f\})$ in one-loop order. For the details we refer to [16].

Due to the different physical input parameters, the mixing angles as well as the neutral current couplings are different in lowest order. This reflects the fact that the separation of $S$ matrix elements into Born terms and radiative corrections is not free of ambiguities. By studying one-loop corrections in either of the schemes, we can get an insight to which extent these contributions compensate the lowest-order differences between both schemes. This will be of special interest in cases where the lowest-order differences become large, for example in the $e^+e^- \to \bar{f}f$ forward-backward asymmetry near the $Z$ resonance. We restrict ourselves to the simplest process $e^+e^- \to \mu^+\mu^-$ in order to exclude additional uncertainties e.g. due to quark fragmentation.

The result of our investigation is that in the critical region around the $Z$ resonance the RS1 and RS2 forward-backward asymmetries are sizable different also after inclusion of one-loop corrections. The polarization asymmetries with weak one-loop corrections are only marginally influenced by the renormalization schemes; however, with QED corrections they are also sizably different in that case.

In Sect. 2 of this paper the renormalization conditions defining both schemes are collated. Section 3 summarizes essential features of the one-loop Green functions, and Sect. 4 contains the comparison of the $M_W - M_Z$ correlation. The integrated cross section and the asymmetries calculated in RS1 and RS2 are discussed in Sect. 5.

## 2. The Schemes

Both schemes are identical with respect to the generation of counterterms yielding finite Green functions. The input parameters $e$, $M_Z$, $M_H$, $\{m_f\}$ are used as free physical parameters in either of the schemes. We list the renormalization condition as follows*:

- The electric charge $e = \sqrt{4\pi\alpha}$ is defined by the nonrelativistic Thomson limit of the Compton scattering.

$$\hat{\Gamma}^{\gamma ee}_\mu(k^2 = 0; \not{p} = \not{q} = m_e) = ie\gamma_\mu. \tag{2.1}$$

- In the limit $k^2 \to 0$ the photon-$Z$-mixing energy has to vanish, i.e. on-shell photons couple to fermions as in pure QED.

$$\mathrm{Re}\,\hat{\Sigma}^{\gamma Z}_T(0) = 0. \tag{2.2}$$

- The residue of the photon propagator is 1:

$$\frac{1}{k^2}\,\mathrm{Re}\,\hat{\Sigma}^{\gamma}_T(k^2)\Big|_{k^2=0} = 0. \tag{2.3}$$

- The physical masses given as the poles of the propagators are equal to their lowest order values by fixing the mass counterterms $\delta M_Z^2$, $\delta M_H^2$, $\{\delta m_f^2\}$ according to

* $\hat{\Sigma}$, $\hat{\Gamma}$ denote renormalized self energies and vertices

$$\mathrm{Re}\,\hat{\Sigma}_T^Z(M_Z^2)=0, \quad \mathrm{Re}\,\hat{\Sigma}^s(M_H^2)=0,$$
$$\mathrm{Re}\,\hat{\Sigma}^f(m_f^2)=0. \tag{2.4}$$

- To determine the wave function renormalization constants, we take into account additional residue conditions:

$$\frac{1}{\not{p}-m_{i-}}\,\mathrm{Re}\,\hat{\Sigma}^{i-}(p)\Big|_{\not{p}=m_{i-}}=0, \tag{2.5}$$

$$\frac{\partial}{\partial p^2}\,\mathrm{Re}\,\hat{\Sigma}^{\eta}(p^2)\Big|_{p^2=M_H^2}=0. \tag{2.6}$$

$i-$ means the $I_3=-1/2$ component of the fermion doublet $i$. In both schemes we have only one renormalization constant for each field multiplet and therefore we are not able to demand a propagator residue 1 for all particles.

The next renormalization condition distinguishes between the two schemes:

*(i) Intermediate Scheme.* This scheme uses the Fermi constant $G_F$ that is related to the muon lifetime $\tau_\mu$ as physical parameter. The numerical value of $\tau_\mu$ is one of the input data and experimentally measured with high precision. It is calculated by considering all electroweak corrections to muon decay. The result can be split into a "weak" four-fermion interaction part with coupling $G_F$ and, on the other side, its electromagnetic corrections which are ultraviolet convergent and gauge invariant. In particular one has up to the first order in the expansion parameter $\alpha$ [17]

$$\tau_\mu^{-1}=G_F^2\frac{m_\mu^5}{192\pi^3}\left(1-8\frac{m_e^2}{m_\mu^2}\right)\left[1+\frac{\alpha}{2\pi}\left(\frac{25}{4}-\pi^2\right)\right] \tag{2.7}$$

and $G_F$ comes out at

$$G_F=1.16634\pm 0.00002\ \ 10^{-5}\,\mathrm{GeV}^{-2}.$$

Taking this condition one gets the relation

$$\frac{G_F}{\sqrt{2}}\leqq\frac{g_2^2}{8M^2}$$

which can be expressed in free parameters as

$$M^2=\frac{1}{2}M_Z^2\left[1+\left(1-\frac{e^2}{\sqrt{2}G_F M_Z^2}\right)^{1/2}\right]. \tag{2.8}$$

$M$ is only used as a book-keeping quantity; it approximates the mass $M_W$ of the charged vector bosons $W^\pm$ in lowest order:

$$M_W=M+\sum_{n=1}^{\infty}M_n\alpha^n. \tag{2.9}$$

Equation (2.7) also supplies us with a 1-loop renormalization condition containing the renormalized $W$ self energy and the renormalization constants $\delta Z_1^W$, $\delta Z_2^W$ for the $SU(2)$ coupling $g_2$ and the gauge field triplet:

$$\mathrm{Re}\left\{\frac{\hat{\Sigma}_T^W(0)}{M^2}+\frac{\alpha}{4\pi}\left(\frac{6}{\sin^2\theta}+\frac{7-4\sin^2\theta}{2\sin^4\theta}\ln\frac{M^2}{M_Z^2}\right)\right.$$
$$\left.+2(\delta Z_1^W-\delta Z_2^W)+\frac{\alpha}{4\pi}\frac{4}{\sin^2\theta}\left(\frac{2}{\varepsilon}-\ln\gamma-\ln\frac{M^2}{4\pi\mu^2}\right)\right\}=0. \tag{2.10}$$

To lowest order the weak mixing angle $\theta$ diagonalizing the $\gamma Z$ mass matrix is given by

$$\cos\theta=\frac{M}{M_Z}. \tag{2.11}$$

*(ii) On-Shell Scheme.* In this scheme the charged vector bosons $W^\pm$ are renormalized on their mass shells. By means of the renormalization condition

$$\mathrm{Re}\,\hat{\Sigma}_T^W(M_W^2)=0 \tag{2.12}$$

the physical mass $M_W$ is incorporated into the scheme as a free and renormalized parameter. It is an essential attribute of the on-shell scheme that it treats the neutral and charged vector bosons identically. We define the Weinberg angle $\theta_W$ by the mass ratio

$$\cos\theta_W=\frac{M_W}{M_Z}. \tag{2.13}$$

Note that the mixing angles are introduced for convenience only. They are no independent parameters in either of the schemes.

As far as the renormalization of the "unphysical" (longitudinal gauge boson, unphysical Higgs, ghost) self energies is concerned, the above list of conditions is not complete. For our purpose of calculating radiative corrections to scattering processes between light fermions ($m_f^2\ll M_W^2$), however, it is sufficient to deal within the framework defined above. We have passed through the complete program but do not give the somewhat lengthy details at this place [12, 18].

## 3. Comparison of Green Functions

Differences between Green functions calculated in both schemes can be traced back to two sources:

(a) The values of parameters like $W$ mass, mixing angle, or neutral couplings are different in both schemes.

(b) The counterterms depend in their finite parts on the renormalization conditions.

The imaginary parts of one-loop self energy- and vertex-functions are finite by themselves and consequently do not give any information about point (b). Therefore we shall discuss only real parts here. For the vector boson self energies, it is convenient to introduce the relative quantities

$$\Pi^{\gamma}=\frac{\mathrm{Re}\,\hat{\Sigma}_T^{\gamma}(k^2)}{k^2}, \qquad \Pi^{\gamma Z}=\frac{\mathrm{Re}\,\hat{\Sigma}_T^{\gamma Z}(k^2)}{k^2}$$
$$\Pi^{W}=\frac{\mathrm{Re}\,\hat{\Sigma}_T^{W}(k^2)}{k^2-M_{(W)}^2}, \qquad \Pi^{Z}=\frac{\mathrm{Re}\,\hat{\Sigma}_T^{Z}(k^2)}{k^2-M_Z^2}. \tag{3.1}$$

The main results can be summarized as follows:
- The photon self energies of the two schemes are nearly identical except of their different thresholds $k^2=4M^2$ resp. $k^2=4M_W^2$ corresponding to the process $\gamma\to W^+W^-$.
- The $W$-boson self energy corrections $\Pi^W$ in the intermediate scheme are generally smaller than those in the on-shell scheme, with the exception of the region around the pole $k^2=M^2$, in which $\Pi_{\mathrm{RS1}}^W$ is ill defined because of non vanishing radiative corrections $\mathrm{Re}\,\hat{\Sigma}_T^W(M^2)\neq 0$. For PETRA energies (40 GeV) we have ($M_Z\leqq 93$ GeV)

$$\Pi_{\mathrm{RS1}}^W\simeq\begin{cases}-0.006; & M_H=10\,\mathrm{GeV}\\ -0.007; & M_H=300\,\mathrm{GeV},\end{cases}$$

$$\Pi_{\mathrm{RS2}}^W\simeq\begin{cases}-0.070; & M_H=10\,\mathrm{GeV}\\ -0.079; & M_H=300\,\mathrm{GeV}.\end{cases}$$

- The counterterms contributing to $\mathrm{Re}\,\hat{\Sigma}_T^Z(k^2)$ are proportional to $(k^2-M_Z^2)$ in both schemes. Thus $\Pi_{\mathrm{RS1}}^Z$ differs from $\Pi_{\mathrm{RS2}}^Z$ mainly by a different renormalization constant $\delta Z_2^Z$. If we chose $M_Z=93$ GeV, we obtain

$$\Pi_{\mathrm{RS1}}^Z-\Pi_{\mathrm{RS2}}^Z\approx 0.07-0.08.$$

In particular for PETRA energies:

$$\Pi_{\mathrm{RS1}}^Z\simeq\begin{cases}+0.003; & M_H=10\,\mathrm{GeV}\\ +0.004; & M_H=300\,\mathrm{GeV},\end{cases}$$

$$\Pi_{\mathrm{RS2}}^Z\simeq\begin{cases}-0.068; & M_H=10\,\mathrm{GeV}\\ -0.076; & M_H=300\,\mathrm{GeV}.\end{cases}$$

- In a similar way, the mixing energy corrections $\Pi_{\mathrm{RS1}}^{\gamma Z}$ and $\Pi_{\mathrm{RS2}}^{\gamma Z}$ are mainly distinguished by a constant around $-0.05$. But now the one-loop corrections are larger in the intermediate scheme. For example, in the PETRA region:

$$\Pi_{\mathrm{RS1}}^{\gamma Z}\simeq\begin{cases}-0.052; & M_H=10\,\mathrm{GeV}\\ -0.055; & M_H=300\,\mathrm{GeV},\end{cases}$$

$$\Pi_{\mathrm{RS2}}^{\gamma Z}\simeq\begin{cases}-0.003; & M_H=10\,\mathrm{GeV}\\ +4\ 10^{-6}; & M_H=300\,\mathrm{GeV}.\end{cases}$$

Consider the neutral couplings

$$v_f=\frac{I_3^f-2Q^f\sin^2\theta}{2\sin\theta\cos\theta}, \qquad a_f=\frac{I_3^f}{2\sin\theta\cos\theta} \tag{3.2}$$

of the $Z$-boson to fermions $f$. In case of $I_3=-1/2$ leptons, the numerator of $v_f$ is small and very sensitive to $\sin^2\theta$. As a consequence, the difference between the mixing angles $\sin^2\theta$ and $\sin^2\theta_W$ is sufficient to make $(v_e)_{\mathrm{RS1}}$ nearly twice as large as $(v_e)_{\mathrm{RS2}}$. The axial vector couplings $a_f$ are not very different in both schemes. The differences in the vector couplings are essentially removed by the $\gamma Z$ mixing energy, whereas the $Z$ self energy leaves the ratio $v_f/a_f$ unchanged.
- Differences between the real one-loop parts of the renormalized gauge-boson fermion vertex functions calculated in our two schemes are smaller than $10^{-3}$ in the range $|k^2|\leqq(150\,\mathrm{GeV})^2$ and are therefore of minor importance.

## 4. The $M_W-M_Z$ Interdependence

*(i) Intermediate Scheme.* Consider the transverse part of the two-point (one-particle irreducible) Green function

$$\Gamma_T^W(k^2)=k^2-M^2+\hat{\Sigma}_T^W(k^2). \tag{4.1}$$

The mass $M_W$ of the charged vector bosons is determined by the zero of $\Gamma_T^W$. This means that the propagator $[\Gamma_T^W(k^2)]^{-1}$ has a pole at the physical mass $k^2=M_W^2$ required by the interpretation of the theory in terms of particles. It should be emphasized that the zero of (4.1) depends on the order of the radiative corrections collected in $\hat{\Sigma}_T^W$. If we substitute (2.9) into (4.1) and take into account only parts up to the first order in $\alpha$, we will find

$$M_W=M+\alpha M_1 \tag{4.2}$$

with

$$\alpha M_1=-\frac{1}{2M}\,\mathrm{Re}\,\hat{\Sigma}_T^W(M^2).$$

The results given by this formula are very close to those determined numerically from (4.1).

*(ii) On-Shell Scheme.* The renormalization condition (2.12) ensures that the parameter $M_W$ has the meaning of the charged vector boson mass. It can be

**Table 1.** The $W$ boson mass $M_W$ in GeV for given masses $M_Z$, $M_H$ (RS: renormalization scheme)

| $M_Z$ (GeV) | RS | $M_H$ (GeV) | | | |
|---|---|---|---|---|---|
| | | 10 | 100 | 300 | 1,000 |
| 88 | 1 | 75.812 | 75.737 | 75.675 | 75.593 |
| | 2 | 75.778 | 75.706 | 75.645 | 75.565 |
| 90 | 1 | 78.387 | 78.314 | 78.253 | 78.172 |
| | 2 | 78.366 | 78.298 | 78.240 | 78.163 |
| 92 | 1 | 80.890 | 80.819 | 80.759 | 80.679 |
| | 2 | 80.880 | 80.814 | 80.757 | 80.683 |
| 93 | 1 | 82.120 | 82.050 | 81.990 | 81.911 |
| | 2 | 82.114 | 82.049 | 81.993 | 81.920 |
| 94 | 1 | 83.338 | 83.268 | 83.208 | 83.130 |
| | 2 | 83.334 | 83.270 | 83.216 | 83.143 |
| 96 | 1 | 85.739 | 85.670 | 85.612 | 85.533 |
| | 2 | 85.742 | 85.679 | 85.625 | 85.554 |
| 98 | 1 | 88.103 | 88.035 | 87.977 | 87.898 |
| | 2 | 88.110 | 88.049 | 87.996 | 87.925 |

used, together with $\alpha$ and the other masses, to calculate the $\mu^-$ lifetime in one-loop order [16]:

$$\frac{1}{\tau_\mu}=\frac{\alpha^2}{384\pi}\frac{m_\mu^5}{(M_W\sin\theta_W)^4}\left(1-8\frac{m_e^2}{m_\mu^2}\right)\cdot\left\{1+2\frac{\hat{\Sigma}_T^W(0)}{M_W^2}+\frac{\alpha}{2\pi}\frac{1}{\sin^2\theta_W}\cdot\left[6+\frac{7-4\sin^2\theta_W}{2\sin^2\theta_W}\ln\frac{M_W^2}{M_Z^2}\right]+\frac{\alpha}{2\pi}\left(\frac{25}{4}-\pi^2\right)\right\}. \quad (4.3)$$

Identifying (4.3) with (2.7), we are able to relate $M_W$ numerically to the parameter set $e$, $G_F$, $M_Z$, $M_H$, and $\{m_f\}$. The value of $M_W$ obtained in this way replaces the directly measured $W$ mass as long as the experimental accuracy of $M_W$ is not comparable with that of $M_Z$.

Table 1 shows $M_W$ for given $Z$ and Higgs masses in the two schemes. The other masses are the same as in [16]. The deviations of both schemes amount between 10 and 50 MeV. Thus they are much smaller than those due to variation of the Higgs mass within each scheme. For the present experimental average of $M_Z=93.0$ GeV the difference is even smaller than 10 MeV if $M_H \leqq 1000$ GeV.

## 5. Comparison of Cross Sections and Asymmetries

We have calculated the virtual 1-loop corrections to the $e^+e^-$ annihilation into muon pairs in both the intermediate and the on-shell scheme. To remove the infrared problem bremsstrahlung diagrams have been taken into account. The resulting *inclusive* cross section is free of infrared divergencies, but it depends on an energy cut $\Delta E/E$ and/or acollinearity cuts. We have used the soft photon approximation [19] and therefore $\Delta E/E=0.1$ will be reasonable. Beside the parameters used in [16], we have chosen the masses

$$M_Z=93\,\text{GeV}, \qquad M_H=100\,\text{GeV}$$

which imply the mixing angles and neutral current couplings given in Table 2.

**Table 2.** Lowest order parameters

| | RS1 | RS2 |
|---|---|---|
| $W$ mass parameter | $M=$ 83.121 | $M_W=$ 82.049 |
| Mixing angle | $\sin^2\theta_0=$ 0.2012 | $\sin^2\theta_W=$ 0.2216 |
| Vector coupling | $v_e=-0.1219$ | $v_e=-0.0683$ |
| Axial vector coupling | $a_e=-0.6237$ | $a_e=-0.6019$ |

### 5.1. Unpolarized Beams

*(i) PETRA Energies.* The differential cross sections calculated in RS1 and RS2 are in excellent agreement for center of mass energies $\sqrt{s}$ lower than 60 GeV. Electromagnetic contributions depend crucially on the experimental cuts. For our $\Delta E/E$, they are the dominant corrections to the Born approximation. Within small deviations, they are the same in both schemes. The weak corrections to $(d\sigma/d\Omega)_{\text{RS1}}$ are vanishingly small. In the on-shell scheme, however, the Born term $\propto a_e^2$ is enhanced by the $Z$ boson energy ($\Theta=\sphericalangle(e^-,\mu^-)$)

$$\frac{\alpha^2}{4s}a_e^2 2\cos\Theta\frac{s}{s-M_Z^2}(1-\text{Re}\,\Pi^Z)\Big|_{\text{RS2}}$$
$$\simeq\frac{\alpha^2}{4s}2a_e^2\cos\Theta\,\text{Re}\frac{s}{s-M_Z^2+\hat{\Sigma}_T^Z(s)}\Big|_{\text{RS2}}$$

with $\Pi^Z$ from (3.1). This is numerically very close to

$$\frac{\alpha^2}{4s}a_e^2\,2\cos\Theta\frac{s}{s-M_Z^2}\Big|_{\text{RS1}}.$$

Table 3 shows the forward-backward asymmetry

$$A_{\text{FB}}(x)\equiv\frac{\int_0^x d\cos\Theta\left(\frac{d\sigma}{d\Omega}\right)-\int_{-x}^0 d\cos\Theta\left(\frac{d\sigma}{d\Omega}\right)}{\int_0^x d\cos\Theta\left(\frac{d\sigma}{d\Omega}\right)+\int_{-x}^0 d\cos\Theta\left(\frac{d\sigma}{d\Omega}\right)} \quad (5.1)$$

and the contributions of the various corrections ($x=1$, $\sqrt{s}=34.5$ GeV).

**Table 3.** The forward-backward asymmetry $A_{FB}$ for $\sqrt{s}$ = 34.5 GeV and $|\cos\Theta| \leqq 1.0$. The bremsstrahlung is included with $\Delta E \leqq 0.1\, E_{beam}$

| | $A_{FB}^{RS1}$ (%) | $A_{FB}^{RS2}$ (%) |
|---|---|---|
| Born | −9.271 | −8.642 |
| Photon self energy (without fermion loops) | +0.0005 | +0.0005 |
| $Z$ self energy | +0.034 | −0.617 |
| $\gamma Z$ mixing | −0.003 | $-5\ 10^{-6}$ |
| Vertex corrections | +0.013 | +0.012 |
| Box diagrams | −0.012 | −0.010 |
| Born + weak | −9.238 | −9.257 |
| QED | +1.904 | +1.744 |
| Full | −7.334 | −7.513 |

*(ii) Integrated Cross Section.* In the energy range $40\,\text{GeV} < \sqrt{s} < 140\,\text{GeV}$ the integrated cross sections of RS1 and RS2, although different in lowest order, agree well after including weak and electromagnetic corrections. This holds especially on resonance $\sqrt{s} = M_Z$, where the difference $\sigma^{RS1} - \sigma^{RS2}$ is smaller than 1 pb.

*(iii) Forward-Backward Asymmetry.* The two forward-backward asymmetries $A_{FB}^{RS1}$ and $A_{FB}^{RS2}$ are plotted as functions of the center of mass energy $\sqrt{s}$ in Fig. 1 (lowest order) and in Fig. 2 (including 1-loop and bremsstrahlung corrections). Obviously the agreement between both schemes is good outside the resonance region. Therefore we shall restrict ourselves to discuss only the resonance region, in particular the interval $I$: $|\sqrt{s} - M_Z| < 10\,\text{GeV}$. In lowest order, $A_{FB}$ can approximately be divided into two components*:

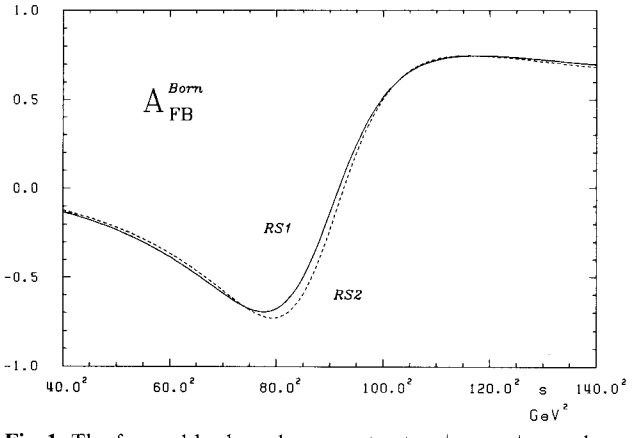


**Fig. 1.** The forward-backward asymmetry to $e^+e^- \to \mu^+\mu^-$ calculated in lowest order in the intermediate scheme (RS1) and the on-shell scheme (RS2)

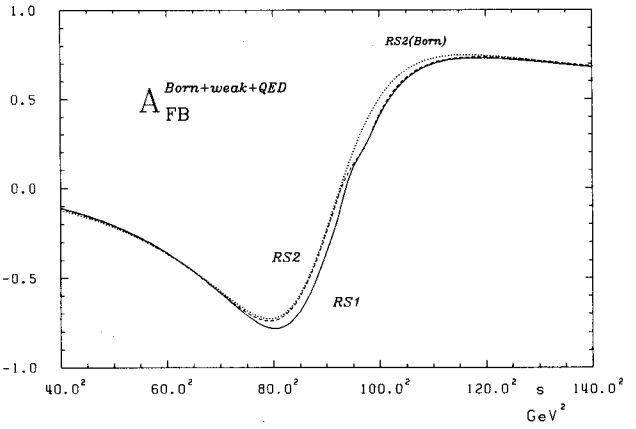


**Fig. 2.** The forward-backward asymmetry with full electroweak one-loop corrections in the schemes RS1 and RS2. The photonic corrections belong to $\Delta E/E = 0.1$. The dotted curve "RS2(Born)" is the on-shell scheme asymmetry in Born approximation, known from Fig. 1

$$A_{FB}^{Born}(x) = \frac{x}{1+\frac{1}{3}x^2}\,\frac{2a^2\,\mathrm{Re}(\chi_0) + 4v^2a^2|\chi_0|^2}{1+2v^2\,\mathrm{Re}(\chi_0) + (v^2+a^2)^2|\chi_0|^2}$$

$$\to A_{FB}^{Born}(x)\Big|_I \simeq \frac{x}{1+\frac{1}{3}x^2}\left\{\frac{2a^2}{1+(v^2+a^2)^2|\chi_0|^2}\,\mathrm{Re}(\chi_0) + \frac{4v^2a^2}{1+(v^2+a^2)^2|\chi_0|^2}\,|\chi_0|^2\right\}. \tag{5.2}$$

Their contributions to the difference of the asymmetries given in both schemes have the same sign below $\sqrt{s} = M_Z$ but opposite signs above. It turns out that the deviation of the RS1 and RS2 curves shown in Fig. 1 vanishes at the upper bound of $I$ and rises smoothly up to maximum value as $\sqrt{s}$ approaches the lower bound.

The main effects of the weak radiative corrections may be understood in terms of the following formula

$$A_{FB}^{Born+weak}|_I \simeq \frac{x}{1+\frac{1}{3}x^2}\cdot\frac{2a^2\,\mathrm{Re}(\chi) + 4v^2a^2\left(1-\frac{2}{v}\,\mathrm{Re}\,\Pi^{\gamma Z}\right)|\chi|^2}{1+(v^2+a^2)^2\left(1-\frac{4v}{v^2+a^2}\,\mathrm{Re}\,\Pi^{\gamma Z}\right)|\chi|^2} \tag{5.3}$$

* The reduced propagators $\chi_0$ are defined as

$$\chi_0(s) = \frac{s}{s - M_Z^2 + iM_Z\Gamma_Z}$$

with the total widths $\Gamma_Z = 2.825\,\text{GeV}$ for RS1 and $\Gamma_Z = 2.562\,\text{GeV}$ for RS2

**Table 4.** The forward-backward asymmetry $A_{FB}$ for $\sqrt{s}$ = 93.0 GeV and $|\cos\Theta| \leqq 1.0$. The bremsstrahlung is included with $\Delta E \leqq 0.1\, E_{beam}$

| | $A_{FB}^{RS1}$ (%) | $A_{FB}^{RS2}$ (%) |
|---|---|---|
| Born | 10.565 | 3.741 |
| Photon self energy (without fermion loops) | −0.0001 | $-2\ 10^{-5}$ |
| $Z$ self energy | ±0.000 | ±0.000 |
| $\gamma Z$ mixing | −8.399 | +0.262 |
| Vertex corrections | −0.514 | −0.245 |
| Box diagrams | −0.090 | −0.075 |
| Born + weak | 1.562 | 3.683 |
| QED | −8.676 | −2.215 |
| Full | −7.114 | 1.468 |

in which the $Z$ self energy is absorbed by correcting $\chi_0$ to

$$\chi(s) = \frac{s}{s - M_Z^2 + \hat{\Sigma}_T^Z(s)}.$$

The dominating contribution to the antisymmetric Re($\chi$) part comes from the $Z$ self energy, while it is the $\gamma Z$ mixing that governs the symmetric $|\chi|^2$ part. Having in mind our comparison of Green functions, the on-resonance asymmetry gets large corrections from the $\gamma Z$ mixing part in the intermediate scheme, whereas in the on-shell scheme the corrections to $A_{FB}(M_Z^2)$ are small. Because of its magnitude, the $\gamma Z$ mixing energy, although yielding

$$v_e^{RS1} \to v_e^{RS1}\left[1 - \frac{1}{v_e}\Pi_{RS1}^{\gamma Z}(M_Z^2)\right] \simeq v_e^{RS2},$$

is not able to correct the *powers* of the neutral vector coupling $v_e^{RS1}$ in (5.3) as good as expected. The seperate corrections of the on-resonance asymmetry are listed in Table 4. The big difference between the lowest order asymmetries $A_{FB}^{RS1}$ and $A_{FB}^{RS2}$ is diminished by inclusion of the weak one-loop corrections, but still a non-negligible difference survices. Taking into account also two-loop contributions to $\mathrm{Im}\,\Sigma^Z$, the results are changed only very slightly (< 0.01 %). The separation between the $A_{FB}$ values becomes even larger if the QED corrections are included:

- The Born resonance term $4v_e^2 a_e^2 2\cos\Theta|\chi|^2$ in the forward-backward asymmetry is proportional to the lowest order vector coupling $v_e^2$, which gets very different values in both schemes. Thus the QED asymmetry corrections of order $\alpha^3$ will show a clear renormalization scheme dependence.
- Furthermore, the QED contributions also decrease the integrated cross section in the denominator of (5.1). All weak corrections to $A_{FB}^{Born}$ will be increased by an amount involved in the value of the QED correction in Table 4.

### 5.2. *Longitudinally Polarized Beams*

With the degrees of longitudinal polarization $P_L^{\pm}$ for $e^{\pm}$ the differential cross section has the form

$$\frac{d\sigma}{d\Omega}(P_L^+, P_L^-) = (1 - P_L^+ P_L^-)\sigma_U(\Theta) + (P_L^+ - P_L^-)\sigma_L(\Theta). \tag{5.4}$$

It is sufficient to discuss the case of electron polarization only: $P_L^+ = 0$, $P_L^- \neq 0$. The observables of interest are:

- the (integrated) polarization asymmetry

$$A_L = \frac{\sigma_L}{\sigma_U}, \quad \sigma_{L,U} = \int d\Omega\, \sigma_{L,U}(\Theta) \tag{5.5}$$

- the forward polarization asymmetry

$$A_L^f = \frac{\sigma_L^f}{\sigma_U^f}, \quad \sigma_{L,U}^f = \int\limits_{\Theta \leqq \pi/2} d\Omega\, \sigma_{L,U}(\Theta) \tag{5.6}$$

- the forward-backward asymmetry $A_{FB}^{pol}$: replace $d\sigma/d\Omega$ in (5.1) by the polarized cross section (5.4).

The integrated polarization asymmetries (5.5) are shown in Figs. 3–5 as functions of $\sqrt{s}$ including successively the weak and QED corrections. The big differences in lowest order are largely removed by inclusion of the weak corrections (Fig. 4). The results after including also the QED corrections, however, are very different: In the on-shell scheme RS2 the corrections are essentially smaller than in RS1; in particular, the radiative tail effect is much more

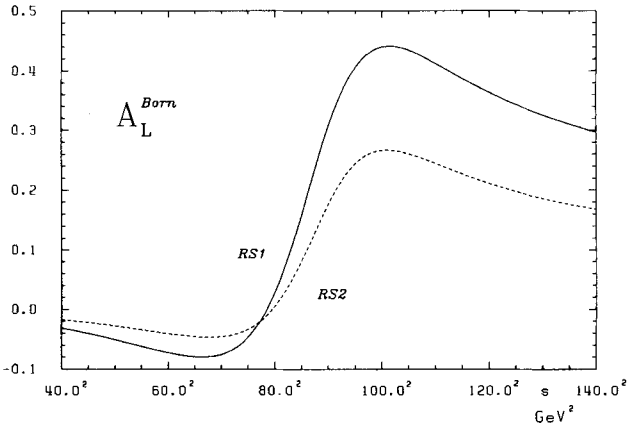


**Fig. 3.** The integrated asymmetry $A_L(e^+e^- \to \mu^+\mu^-)$ in lowest order. RS1 and RS2 denote the renormalization schemes underlying the curves

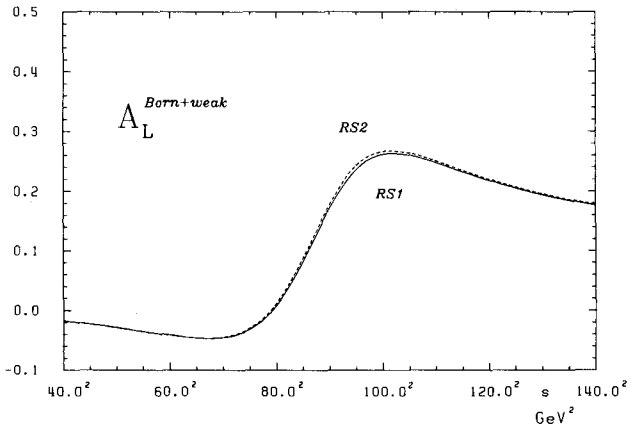


**Fig. 4.** The integrated asymmetry $A_L(e^+e^- \to \mu^+\mu^-)$ after taking into account the weak one-loop corrections

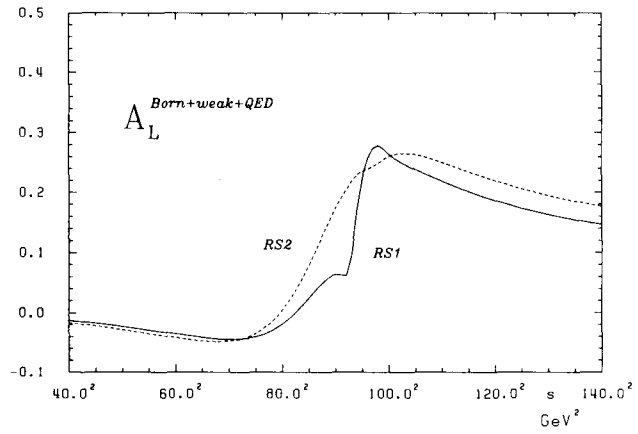


**Fig. 5.** The one-loop corrected integrated asymmetry $A_L(e^+e^- \to \mu^+\mu^-)$. The photonic contributions belong to $\Delta E/E = 0.1$

pronounced in RS1. This behaviour can be understood by the fact that the QED corrections to the unpolarized ($\sigma_U$) and the polarized ($\sigma_L$) parts of the cross section are rather big, but they cancel largely in the ratio $A_L = \sigma_L/\sigma_U$ in RS2. In RS1 this cancellation does not work since the Born values are too much different.

In Table 5 we put together the on-resonance values for the various asymmetries $A_L$, $A_L^f$ and $A_{FB}^{pol}(P_L^- = -1)$. It can be seen that the corrections (weak as well as QED) are rather small in the on-shell scheme but large in RS1.

The size of our given values for the QED corrections (polarized and unpolarized) was derived from the specific choice of $\Delta E/E = 0.1$. For realistic experimental situations, however, other cuts needing also the complete hard bremsstrahlung part may be more appropriate. The quantitative results with such QED corrections will in general be different from

**Table 5.** The integrated asymmetries $A_L$, $A_L^f$, $A_{FB}^{pol}$ for $\sqrt{s} = 93.0$ GeV and $|\cos\Theta| \leqq 1.0$. The bremsstrahlung is included with $\Delta E \leqq 0.1\, E_{beam}$

| | RS | Born | Born + weak | Full |
|---|---|---|---|---|
| $A_L$ | 1 | 37.427 | 21.429 | 9.540 |
| (%) | 2 | 22.271 | 22.222 | 21.893 |
| $A_L^f$ | 1 | 59.238 | 36.904 | 17.816 |
| (%) | 2 | 37.569 | 37.489 | 37.671 |
| $A_{FB}^{pol}(P_L^- = -1)$ | 1 | 28.113 | 14.505 | −0.096 |
| (%) | 2 | 16.721 | 16.635 | 14.602 |

our values. However, the qualitative result that they are influenced by the electroweak renormalization scheme should show up also in other experimental situations.

In conclusion, we have investigated the renormalization scheme dependence of one-loop electroweak corrections by means of two different schemes explicitly specified. We have found that the relation between $M_W$ and $M_Z$ is practically the same in both schemes. Also the integrated cross section and the forward-backward asymmetry for $e^+e^- \to \mu^+\mu^-$ at PETRA energies are quantities which essentially do not depend on the choice of a specific scheme. For the forward-backward asymmetry around the $Z$, in particular the on-resonance asymmetry, however, strikingly different predictions are obtained according to the underlying renormalization scheme. The polarization asymmetries show a much weaker scheme dependence as far as only the weak corrections are included; the QED corrections again deviate considerably from each other.

The presence of large scheme dependence effects signals need of next order contributions. Since the one-loop corrections to the asymmetries are relatively small in the on-shell scheme (very small for polarization asymmetries) it seems a reasonable assumption that next order effects will play only a subordinate role in RS2. This conjecture is supported by the fact that the inclusion of the $\gamma - Z$ mixing in the bremsstrahlung (virtual + real) diagrams absorbs the main part of the deviations in the QED corrections and brings the RS1 near to the RS2 result. In order to get a finally satisfactory answer more systematic studies on the next order contributions will be necessary.

## References

1. S.L. Glashow: Nucl. Phys. **22**, 579 (1961); S. Weinberg: Phys. Rev. Lett. **19**, 1264 (1967); A. Salam: in Elementary Particle Physics, N. Svartholm, ed., p. 367. Stockholm: Almquist and Wiksell, 1968
2. UA1 Collab. G. Arnison et al.: Phys. Lett. **126B**, 398 (1983);

UA2 Collab. P. Bagnaia et al.: Phys. Lett. **129B**, 130 (1983); UA1 Collab. G. Arnison et al.: CERN-EP/83-162 (1983) [3]
3. G. 't Hooft: Nucl. Phys. **B33**, 173 (1971); Nucl. Phys. **B35**, 165 (1971)
4. D.A. Ross, J.C. Taylor: Nucl. Phys. **B51**, 125 (1973); Nucl. Phys. **B58**, 643(E) (1973); S. Sakakibara: Phys. Rev. **D24**, 1149 (1981); E.A. Paschos, M. Wirbel: Nucl. Phys. **B194**, 189 (1982)
5. K.I. Aoki et al.: Suppl. Prog. Theor. Phys. **73**, 1 (1982)
6. A. Sirlin: Phys. Rev. **D22**, 971, (1980); W.J. Marciano, A. Sirlin: Phys. Rev. **D22**, 2695 (1980)
7. M. Green, M. Veltman: Nucl. Phys. **B169**, 137 (1980); Nucl. Phys. **B175**, 547(E) (1980)
8. F. Antonelli, M. Consoli, G. Corbo: Phys. Lett. **91B**, 90 (1980); F. Antonelli, G. Corbo, M. Consoli, O. Pellegrino: Nucl. Phys. **B183**, 195 (1981)
9. C.H. Llewellyn Smith, J.F. Wheater: Phys. Lett. **105B**, 486 (1981); J.F. Wheater, C.H. Llewellyn Smith: Nucl. Phys. **B208**, 27 (1982)
10. G. Passarino, M. Veltman: Nucl. Phys. **B160**, 151 (1979); M. Consoli: Nucl. Phys. **B160**, 208 (1979)
11. J. Fleischer, F. Jegerlehner: Phys. Rev. **D23**, 2001 (1981); W. Wetzel: Nucl. Phys. **B227**, 1 (1983); J. Cole: in [14]; M. Böhm, W. Hollik: Phys. Lett. **139B**, 213 (1984); W. Hollik: Phys. Lett. **152B**, 121 (1985); R.W. Brown, R. Decker, E.A. Paschos: Phys. Rev. Lett. **52**, 1192 (1984); B.W. Lynn, R.G. Stuart: Nucl. Phys. **B253**, 216 (1985); M. Böhn, A. Denner, W. Hollik, R. Sommer: Phys. Lett. **144B**, 404 (1984)
12. M. Böhm, W. Hollik, H. Spiesberger: DESY 84-027 (1984) (Fortschr. Phys., to be published)
13. S. Sakakibara: Z. Phys. C – Particles and Fields **11**, 43 (1981)
14. B.W. Lynn, J.F. Wheater, eds.: Workshop on Radiative Corrections in $SU(2)_L \times U(1)$, Miramare, Trieste 1983. Singapore: World Scientific 1984
15. J. Ellis, R. Peccei, eds.: Physics at LEP, CERN 86-02 (1986) 86-02 (1986)
16. M. Böhm, W. Hollik, H. Spiesberger: Z. Phys. C – Particles and Fields **27**, 523 (1985)
17. R.E. Behrends, R.J. Finkelstein, A. Sirlin: Phys. Rev. **101**, 866 (1956); S.M. Berman: Phys. Rev. **112**, 267 (1958); T. Kinoshita, A. Sirlin: Phys. Rev. **113**, 1652 (1959)
18. H.-J. Timme: Diplomarbeit, Univ. Hamburg (1985)
19. M. Böhm, W. Hollik: Nucl. Phys. **B204**, 45 (1982); Z. Phys. C – Particles and Fields **23**, 31 (1984)